ACS OMEGA

Open Access

http://pubs.acs.org/journal/acsodf

Article

Electrode-Supported Protonic Ceramic Electrolysis Cells for Electrochemically Promoted Ammonia Synthesis at Intermediate Temperatures

Moe Okazaki and Junichiro Otomo*

Cite This: *ACS Omega* 2023, 8, 40299−40308

Read Online

ACCESS | Metrics & More | Article Recommendations | Supporting Information

ABSTRACT: Protonic ceramic electrolysis cells (PCECs) have attracted attention for their applications in electrochemical ammonia synthesis, but their low Faradaic efficiency and thermodynamic constraints at high operating temperatures have led to low ammonia formation rates. In this work, electrode-supported PCECs with a noble-metal-free Ni-$BaZr_{0.8}Y_{0.2}O_{3-\delta}$ cathode and a spin-coated proton-conducting electrolyte were developed for ammonia electrosynthesis, conducted in a single-chamber reactor cofed with N_2 and H_2. Ammonia formation rates increased non-Faradaically with applied voltage, reaching up to 1.1 × 10^{-8} mol s^{-1} cm^{-2} at 400 °C, which corresponds approximately to a 150 °C reduction in operating temperature compared to previously reported works conducted in mixed N_2 and H_2. The improved performance at intermediate temperatures by using a Ni catalyst is attributed to the electrochemical promotion of catalysis upon cathodic polarization. By fabrication of a cell with low Ohmic losses and improved contact resistance at the anode−electrolyte interface, sufficient cathodic polarization to accelerate ammonia formation was achieved, even at 400 °C. A combined water electrolysis and ammonia synthesis system is proposed, where the hydrogen byproduct from water electrolysis can be efficiently utilized via a recycling process; such a system requires enhanced ammonia formation in a mixed N_2/H_2 atmosphere, as demonstrated in this work.

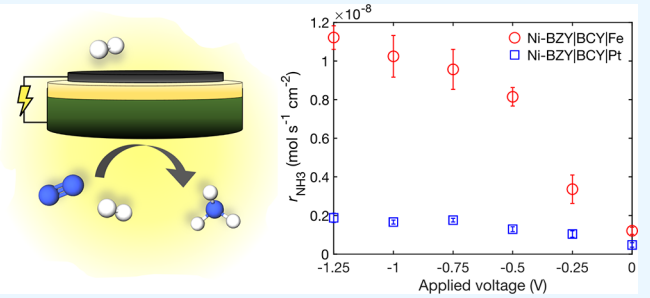

1. INTRODUCTION

Ammonia is an essential chemical that has been used globally in fertilizers and has recently attracted further attention for its use as an energy carrier. It can be easily liquefied at just 8 bar at standard temperatures, forming a fuel with high volumetric energy and hydrogen density. Industrially, ammonia is produced via the Haber−Bosch process; however, the use of fossil fuel-derived hydrogen causes the process to contribute to 1.2% of global CO_2 emissions.[1,2] Moreover, the large scale of production, intensive conditions, and long start-up times required to condition the Fe-based catalysts[3] make it difficult to integrate into intermittent renewable energy-based production systems.

An alternative to the Haber−Bosch process is ammonia electrosynthesis: electrochemically converting water and nitrogen into ammonia, ideally powered by renewable energy. Ammonia electrosynthesis has been conducted across temperatures ranging from ambient conditions to around 700 °C, using electrochemical cells with either aqueous solutions, alkaline membranes, polymer electrolyte membranes, solid acids, molten salts, or proton-conducting ceramics as electrolytes.[4,5]

In this work, we focus on protonic ceramic electrolysis cells (PCECs), typically used for ammonia electrosynthesis in the high-temperature regime above 500 °C. With proton-conducting electrolytes, ammonia electrosynthesis proceeds as follows: water dissociates to form protons and electrons at the anode side (eq 1), and then the protons and electrons are conducted through the electrolyte and the external circuit, respectively, to reach the cathode side, where they finally react with nitrogen to form ammonia (eq 2). The overall reaction is shown in eq 3:

$$\frac{3}{2}H_2O \rightarrow 3H^+ + 3e^- + \frac{3}{4}O_2 \quad (1)$$

$$\frac{1}{2}N_2 + 3H^+ + 3e^- \rightarrow NH_3 \quad (2)$$

$$\frac{3}{2}H_2O + \frac{1}{2}N_2 \rightarrow NH_3 + \frac{3}{4}O_2 \quad (3)$$

Received: June 23, 2023
Revised: August 26, 2023
Accepted: September 26, 2023
Published: October 19, 2023

However, a competing reaction simultaneously occurs at the cathode side: the protons and electrons may undesirably recombine, forming hydrogen gas instead (eq 4). This results in a low Faradaic efficiency, which represents how well the current flowing through the cell is used to form ammonia. A low Faradaic efficiency directly reduces the energy efficiency of typical ammonia electrosynthesis systems:

$$2H^+ + 2e^- \rightarrow H_2 \quad (4)$$

Another challenge faced in ammonia electrosynthesis using PCECs is that at high temperatures, the equilibrium conversion of nitrogen to ammonia decreases with temperature. In addition, from a system point of view, lower operating temperatures are essential for compatibility with daily start-and-stop operation to match the fluctuating output of renewable energy-based power generation systems.

To address these issues of low Faradaic efficiency and low conversion using PCECs at high temperatures, we propose a system that implements hydrogen recycling and operates at intermediate temperatures. Typically, ammonia electrosynthesis is conducted with pure N_2 gas fed to the cathode side, as described above. However, the H_2 byproduct generated at the cathode side (eq 4) can be recycled back to the cathode inlet gas stream, creating a mixed N_2/H_2 cathodic gas feed. Under such conditions, ammonia can also be synthesized catalytically (eq 5):

$$\frac{1}{2}N_2 + \frac{3}{2}H_2 \rightarrow NH_3 \quad (5)$$

Ammonia electrosynthesis under such cofed N_2/H_2 conditions has led to enhanced ammonia formation rates,[6−10] including a 30-fold enhancement compared to that in pure N_2.[9] Our group reported that high ammonia formation rates in the order of 10^{-8} mol s^{-1} cm^{-2} are possible in dry N_2/H_2 under cathodic polarization, even with low current densities in the order of 10 mA cm^{-2}.[8] The ammonia formation rate was shown to depend more on the cathodic polarization than on the current density, meaning that the Faradaic efficiency is less critical for the amount of ammonia synthesized. These enhancements have been attributed to the electrochemical promotion of catalysis (EPOC),[11,12] which has also been referred to as the non-Faradaic electrochemical modification of catalytic activity.[13,14] In EPOC-based processes, high ammonia formation rates can be achieved without the use of noble metal catalysts, using catalysts such as Fe and Ni instead. Furthermore, by use of a dry cathodic gas feed, the produced ammonia does not have to be separated from water, eliminating the energy required for separation. However, as electrochemical promotion of ammonia synthesis has only been evident above 500 °C, its viability at intermediate temperatures remains unknown.

Recently, intermediate temperature ammonia electrosynthesis has been focused on, owing to the balance between thermodynamic favorability and kinetic considerations.[15] To operate PCECs efficiently at intermediate temperatures, electrode-supported cells with a thin electrolyte layer should be considered to minimize Ohmic losses upon proton conduction through the electrolyte. The conductivity values of the best protonic ceramic electrolytes are in the order of 10^{-2}−10^{-3} S cm^{-1} at 600 °C,[16,17] but this declines notably with temperature. Despite this bottleneck, most PCECs for ammonia electrosynthesis feature thick electrolyte supports. Several exceptions have demonstrated the use of electrode-supported cells,[6,10,18−20] including a recent study reporting exceptionally high ammonia formation rates up to 8×10^{-8} mol s^{-1} cm^{-2} using Ru-infiltrated catalysts in wet N_2.[20] A few of these studies using PCECs are conducted with cofed hydrogen;[6,10] however, only comparatively low ammonia formation rates up to 1×10^{-9} mol s^{-1} cm^{-2} have been reported below 500 °C in mixed N_2/H_2.[7]

In this work, we evaluate the behavior of noble-metal-free electrode-supported PCECs with a Ni-$BaZr_{0.8}Y_{0.2}O_{3-\delta}$ (Ni-BZY) cermet cathode support and a thin $BaCe_{0.9}Y_{0.1}O_{3-\delta}$ (BCY) electrolyte to conduct electrochemical promotion of catalysis at intermediate temperatures. To replicate the behavior of the cathode in a recycled gas feed, experiments are conducted in a single-chamber reactor with a mixed N_2/H_2 atmosphere, which, as we previously demonstrated using electrolyte-supported cells, can lead to the observation of electrochemical promotion.[21] Both Pt and Fe were tested as anodes to analyze the influence of Ohmic, anodic, and cathodic resistances on the electrochemical ammonia formation, using electrochemical impedance spectroscopy (EIS). Using a Ni catalyst for ammonia synthesis, we report high ammonia formation rates up to 1.1×10^{-8} mol s^{-1} cm^{-2} at 400 °C, which are achieved by a cell design that enhances the cathodic polarization under applied voltage. We show that PCECs can be a contender for ammonia electrosynthesis even at intermediate temperatures, given the following three features: (1) cathodic gas feed of mixed nitrogen and hydrogen to enable the electrochemical promotion of catalysis upon cathodic polarization; (2) thin electrolyte to limit Ohmic resistance; and (3) anode material with low interfacial charge transfer resistance to limit Ohmic and anodic resistances. Such enhanced ammonia formation in N_2/H_2 at intermediate temperatures is promising for the development of a novel ammonia electrosynthesis system that combines water electrolysis and ammonia synthesis based on the electrochemical promotion of catalysis via hydrogen recycling.

2. RESULTS AND DISCUSSION

2.1. Characterization. Figure 1 shows X-ray diffraction (XRD) patterns of the synthesized BCY powder, spin-coated BCY electrolyte after cosintering, and reduced Ni-BZY support after electrochemical measurements. Perovskite phase peaks attributed to either BCY or BZY are seen in all samples. Two major Ni peaks are seen for the Ni-BZY support. A minor NiO peak is seen in the BCY spin-coated surface, likely from the as-sintered NiO-BZY support beneath. A minor impurity is observed in the reduced Ni-BZY support and is assigned to Pt(111), likely due to the Pt electrode pasted on the other side of the cell.

Figure 2 shows the cross-sectional field emission scanning electron microscopy (FE-SEM) results of electrode-supported Ni-BZY | BCY | Pt and Ni-BZY | BCY | Fe cells after reduction and electrochemical measurements, all taken in the back-scattered electron mode. In both cells, the Ni-BZY support has adequate porosity, and the spin-coated electrolyte is observed to be dense and crack-free, aside from some pinholes. The electrolyte thicknesses are approximately 10 μm in both cells. The formation of a separate microstructure is observed at the Fe-BCY interface (Figure 2f), which is not observed at the Pt-BCY interface (Figure 2c). We previously reported that a similar interfacial layer forms during the sintering of an Fe_2O_3 electrode on a BCY electrolyte support. We showed, using electron probe microanalysis (EPMA), that this was a result of

https://doi.org/10.1021/acsomega.3c04478
ACS Omega 2023, 8, 40299−40308

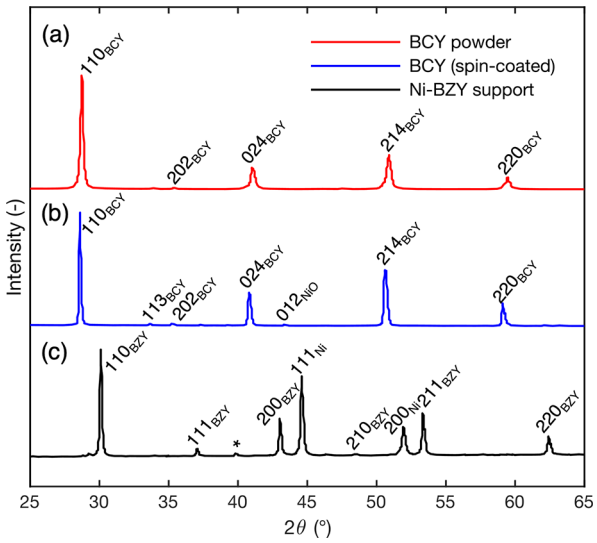

Figure 1. XRD patterns of BCY powder, spin-coated BCY electrolyte, and Ni-BZY electrode support after sintering and reduction. *: Pt(111) impurity.

cation interdiffusion at the interface, and that the interfacial layer is comprised mainly of ceria.[21] This interdiffusion appears to occur when the cations in the oxide can hold multiple oxidation states.[22] Furthermore, we observed upon handling the cells that the Fe anode appears to have stronger adhesion to the electrolyte than the Pt anode does, which we believe is a result of this interfacial cation interdiffusion.

2.2. Electrochemical Impedance Spectroscopy. Figure 3a,b shows the Nyquist plots of electrode-supported cells in 50% N_2/50% H_2 at 400 °C, taken under open-circuit voltage (OCV) conditions. Both EIS spectra were fitted to the equivalent circuit shown in Figure 3c, consisting of an inductor (L), a resistor (R_{Ohm}), and two pairs of resistors and constant phase elements (CPEs) in parallel, labeled as high-frequency (HF) and low frequency (LF). The parameters used to fit the data are listed in Table 1. CPEs are expressed using their pseudocapacitance Q, resulting in an impedance denoted by $Z = 1/(j\omega)^n Q$, where n takes a value between 0 and 1. The equivalent capacitance C is calculated by $C = (QR)^{1/n}/R$.

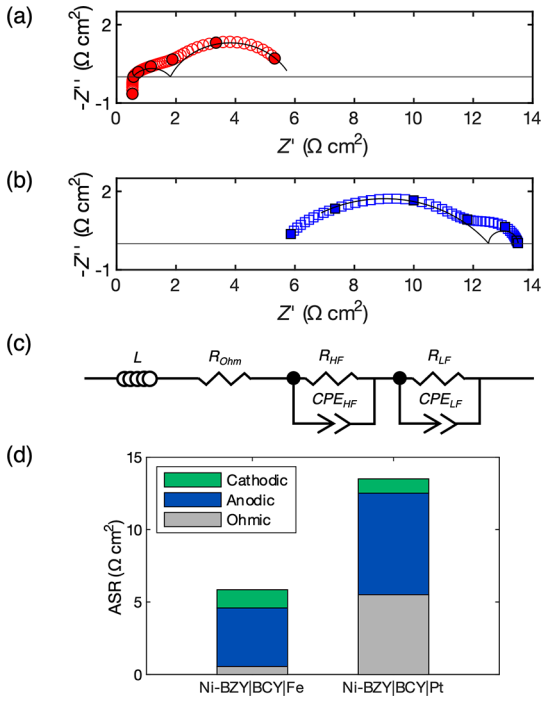

Figure 3. Electrochemical impedance spectra of (a) Ni-BZY | BCY | Fe and (b) Ni-BZY | BCY | Pt cells taken at 400 °C under the OCV conditions. Open circles indicate raw data points, filled circles denote raw data points at every decade (10^5–10^{-1} Hz), and solid lines show calculated fitting for individual semicircles. (c) Equivalent circuit used for fitting. (d) Breakdown of ASR values.

The R-CPE semicircles of the Ni-BZY | BCY | Pt cell and Ni-BZY | BCY | Fe cell are assigned to physical phenomena based on comparisons between the two cells and to literature.[23,24] The attribution of EIS elements is difficult in a single chamber, as both the anode and cathode would be affected by any variations in the atmosphere. Instead, as the two cells are fabricated and tested in the same way aside from the anode, we used this comparison to determine that the cathodic elements should be similar, while the anodic elements may vary between the two cells. R-CPE elements with frequencies on the order of 10 Hz, which appear in both

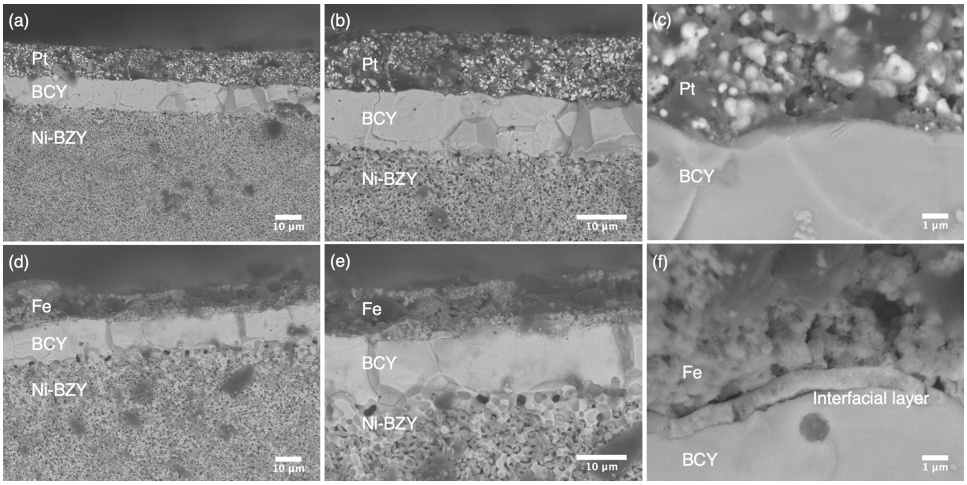

Figure 2. Cross-sectional FE-SEM micrographs of electrode-supported cells (a–c) Ni-BZY | BCY | Pt and (d–f) Ni-BZY | BCY | Fe, all taken in backscattered electron mode after electrochemical measurements.

https://doi.org/10.1021/acsomega.3c04478
ACS Omega 2023, 8, 40299−40308

Table 1. Fitting Parameters for EIS Data of Electrode-Supported Cells at OCV

	Ni-BZY | BCY | Fe	Ni-BZY | BCY | Pt
L (H cm^2)	1.1×10^{-6}	2.7×10^{-7}
R_{Ohm} (Ω cm^2)	0.55	5.50
component	cathode (HF)	cathode (LF)
f (Hz)	74	18
R_C (Ω cm^2)	1.26	0.99
Q_C (F s^{n-1} cm^{-2})	2.0×10^{-2}	9.4×10^{-3}
n_C (−)	0.60	0.99
C_C (F cm^{-2})	1.7×10^{-3}	8.9×10^{-3}
component	anode (LF)	anode (HF)
f (Hz)	0.7	2214
R_A (Ω cm^2)	4.04	7.02
Q_A (F s^{n-1} cm^{-2})	8.7×10^{-2}	5.7×10^{-4}
n_A (−)	0.73	0.58
C_A (F cm^{-2})	5.8×10^{-2}	1.0×10^{-5}

cells, are attributed to gas diffusion in the Ni-BZY cathode support. They have similar equivalent capacitance values in the order of 10^{-3} F cm^{-2} and similar resistances of approximately 1 Ω cm^2. On the contrary, the anodic CPE elements vary significantly and are therefore likely due to different physical phenomena. The R-CPE element at 2214 Hz is assigned to the charge transfer resistance in the Pt anode and at the Pt/BCY interface. The second CPE element for Ni-BZY | BCY | Fe is at a low frequency (0.7 Hz), which suggests that it is due to gas diffusion and effects of chemical capacitance at the Fe anode;[23,25] unlike Pt, Fe is not a common anode material and is poor at dissociating H_2 into H^+.

The contributions of each resistive element to the overall area-specific resistance (ASR) are summarized in Figure 3d. For simplicity, the anodic Pt charge transfer resistance and the anodic Fe gas diffusion/chemical capacitance contribution are shown in the same color. By implementing Fe as the anode, the Ohmic and anodic resistances both decreased, while the cathodic resistance remained similar between the two cells. The reduction of the Ohmic and anodic resistances is likely due to improved contact resistance at the anode, associated with the formation of the interfacial layer observed in Figure 2f. High contact resistance at the electrode−electrolyte interface (in particular, with the electrode sintered at low temperatures, which in electrolysis is the anode) has indeed been the focus of recent protonic ceramic fuel cell (PCFC) works.[16,26] Furthermore, the reduction of Ohmic resistance may be in part due to the introduction of partial electronic conductivity, as mixed ionic-electronic conductivity has been reported in Fe-doped barium-based perovskites.[27,28] Overall, the contribution of the cathodic resistance to the total resistance increased from 7% in the Ni-BZY | BCY | Pt cell to 22% in the Ni-BZY | BCY | Fe cell.

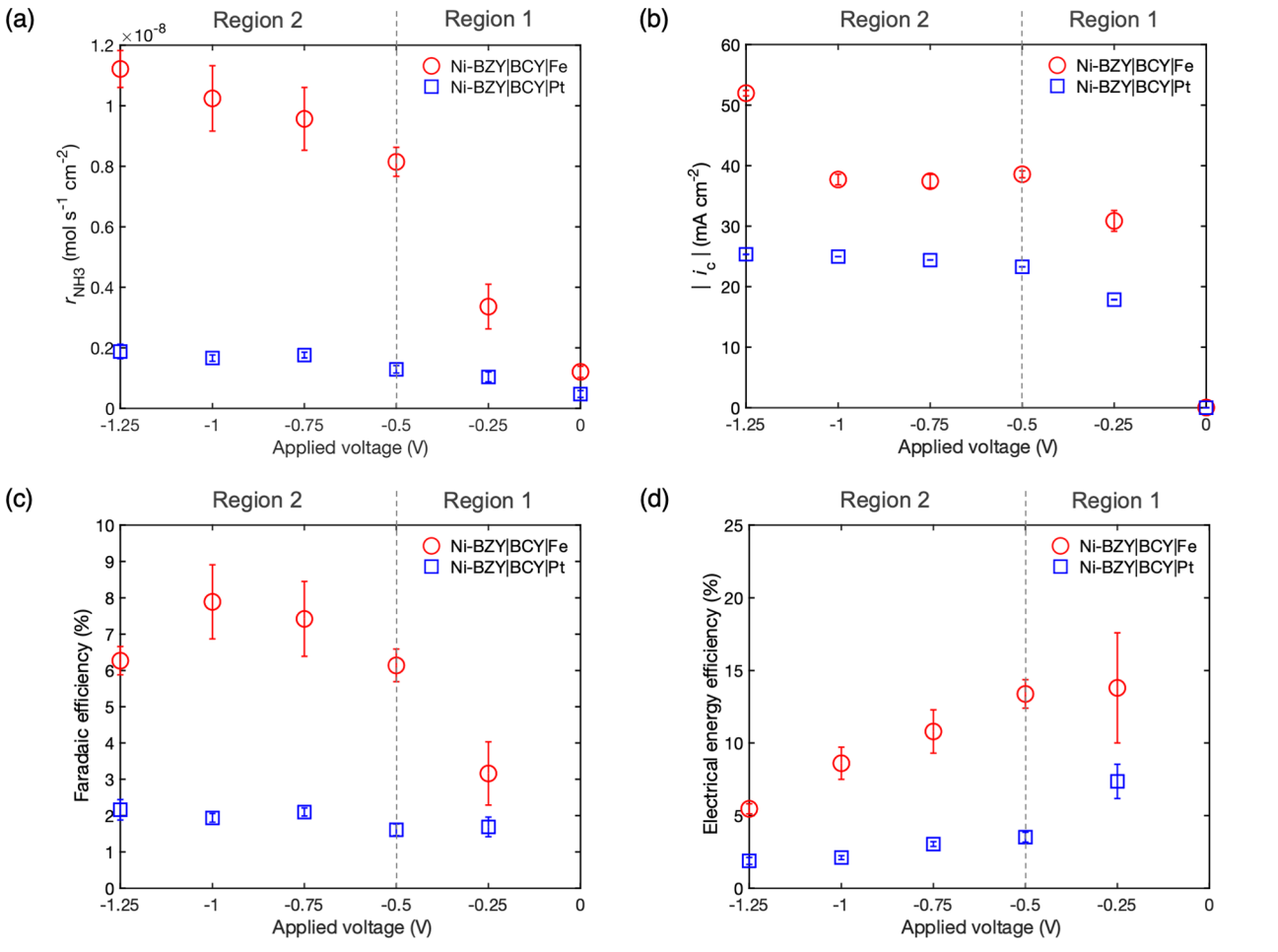

Figure 4. Effect of applied voltage on the (a) ammonia formation rate normalized by electrode area, (b) current density, (c) Faradaic efficiency, and (d) electrical energy efficiency of electrode-supported Ni-BZY | BCY | Pt and Ni-BZY | BCY | Fe cells.

https://doi.org/10.1021/acsomega.3c04478
ACS Omega 2023, 8, 40299−40308

2.3. Electrochemical Ammonia Synthesis. Results of electrochemical ammonia synthesis at 400 °C in 50% N_2/50% H_2, using the two types of electrode-supported cells, Ni-BZY | BCY | Pt and Ni-BZY | BCY | Fe, are shown in Figure 4. The ammonia formation rate (r_{NH3}) and current density (i_c) are normalized by the electrode area. For each r_{NH3} data point, the average and standard deviation across the four liquid chromatography measurements are plotted, while the current density was measured throughout the ammonia collection period. The Faradaic efficiency and the electrical energy efficiency are defined by eqs 6 and 7, respectively, where n is the number of electrons, F is the Faraday constant, V is applied voltage, M_{NH3} is the molar mass of NH_3, and LHV_{NH3} is the lower heating value of NH_3:

$$\mathrm{FE} = \frac{r_{NH3}}{i_c/nF} \tag{6}$$

$$\text{Electrical energy efficiency} = \frac{r_{NH3}}{i_c V} M_{NH3} \mathrm{LHV}_{NH3} \tag{7}$$

The total ammonia formation rates, including any catalytic contributions, are used to calculate Faradaic and electrical energy efficiencies. Standard deviations for the ammonia formation rate and current density are propagated to obtain standard deviation values for the Faradaic and electrical energy efficiencies.

The ammonia formation rates at the OCV, due to the catalytic reaction according to eq 5, are relatively low in both cells, on the order of 1×10^{-9} mol s^{-1} cm^{-2}, as shown in Figure 4a. As a voltage is applied, the ammonia formation rates increase in both cells. With the Ni-BZY | BCY | Fe cell, a high ammonia formation rate of 1.1×10^{-8} mol s^{-1} cm^{-2} was obtained at −1.25 V, which marks a 10-fold improvement compared to that obtained at OCV. With the Ni-BZY | BCY | Pt cell, the ammonia formation rate increases only slightly with applied voltage, plateauing at only 2×10^{-9} mol s^{-1} cm^{-2} at around −0.75 V. Both the ammonia formation rate and the current density are higher for the Ni-BZY | BCY | Fe cell at all applied voltages.

The relationship between the ammonia formation rates and current densities of the Ni-BZY | BCY | Pt and Ni-BZY | BCY | Fe cells also varies significantly. Figures 4a,b show that while the ammonia formation rate varies by up to 5-fold between the two cells, the current density is only two times greater. This comparison indicates that the acceleration of ammonia formation in the Ni-BZY | BCY | Fe cell cannot be accounted for by just the increased current density. Instead, these results suggest that electrochemical promotion is enabled by a direct effect of the applied voltage, which agrees with previously reported results of ammonia formation based on EPOC.[8] Although the ammonia formation reaction takes place at the same Ni-BZY cathode, the two cells exhibit different anodic and Ohmic resistances, as demonstrated by Figure 3. By limiting the anodic and Ohmic resistances in the Ni-BZY | BCY | Fe cell, it appears that a larger cathodic polarization can be achieved, thereby promoting ammonia formation. By varying the anodic material, the cathodic polarization is tuned indirectly, without simultaneously changing the catalytic activity or selectivity of the cathodic material.

The electrochemical behavior of the Ni-BZY | BCY | Fe cell is discussed herein in terms of two separate regions of applied voltage, as indicated in Figure 4. In Region 1, between 0 and −0.5 V, the ammonia formation rate appears to increase exponentially, reaching 8.1×10^{-9} mol s^{-1} cm^{-2}. An exponential increase in ammonia formation rate was also observed in our previous study using an iron-impregnated electrode in mixed N_2/H_2 at 610 °C.[9] In Region 1, the current density also increases but less steeply than the ammonia formation rate does. As a result, the Faradaic efficiency increases notably with applied voltage, as seen in Figure 4c. In typical ammonia electrosynthesis, the ammonia formation rate is proportional to the current density as the protons conducted through the electrolyte are the only source of hydrogen atoms available to form ammonia. However, the Ni-BZY | BCY | Fe cell exhibits non-Faradaic behavior, which aligns with our previous reports on non-Faradaic ammonia electrosynthesis using electrolyte-supported cells, both in double-chamber[8,9] and single-chamber[21] reactors. The difference in Faradaic efficiency between the two cells and the non-Faradaic behavior are both likely attributed to the aforementioned effect of cathodic polarization. As the ammonia formation rate is dependent not only on the current density but also on the voltage applied to the cathode, the Faradaic efficiencies differ despite the electrolyte being the same. Although the overall Faradaic efficiency is relatively low in this work compared to that of other EPOC-based works, the Faradaic efficiency increases notably with applied voltage, still resulting in the observation of non-Faradaic behavior in these electrode-supported cells.

In Region 2, the current density remains unchanged between −0.5 and −1.0 V. This limiting current density in this regime is likely due to inadequate electrode fabrication, such as maintaining sufficient porosity at the electrode/electrolyte interfaces, and is expected to be improved by further efforts in cell fabrication. Regardless, the ammonia formation rate continued to increase. The current-independent behavior of ammonia synthesis also indicates non-Faradaic promotion. Nevertheless, the ammonia formation rate appears to saturate between −0.5 and −1.25 V. This saturation was also observed when using a pure iron catalyst on an electrolyte-supported cell at 550 °C in mixed N_2/H_2.[8] The highest ammonia formation rate of 1.1×10^{-8} mol s^{-1} cm^{-2} is equivalent to a partial pressure p_{NH3} of 5×10^5 atm, which corresponds to just 1.5% of the equilibrium ammonia composition that is thermodynamically expected under these experimental conditions. However, the geometry of the single-chamber reactor is such that the active cell area is less than 10% that of the quartz tube cross-section (details in Methods). This would cause some of the gas to flow past the cell unreacted. Therefore, it is possible that the ammonia concentration calculated based on the total gas flow rate is an underestimation and that the actual ammonia concentration within the electrode is much higher. As a result of the saturation, the electrical energy efficiency decreases with applied voltage beyond −0.5 V, as shown in Figure 4d. This metric is used here to evaluate how effectively the electrical power applied to the cell is converted into ammonia without accounting for the enthalpy of the hydrogen gas feed as input energy. When considering both the ammonia formation rate and the electrical energy efficiency, −0.5 V appears to be a suitable operating condition. Based on the trends seen in Region 2, it is likely that even if the ammonia formation rate increases slightly at applied voltages above −1.25 V, the overall efficiency of the cell would only continue to decrease.

To eliminate the possible effects of adventitious sources of nitrogen species in the experimental environment,[29] back-

https://doi.org/10.1021/acsomega.3c04478
ACS Omega 2023, 8, 40299−40308

ground measurements (50% H_2/Ar with applied voltage) were conducted (Figure S1). The reversibility and stability of the high electrochemical enhancement are shown in Figures S2 and S3. Furthermore, the results of a second Ni-BZY | BCY | Fe cell are shown in Figure S4 to demonstrate the reproducibility of these results. Finally, to validate the result of the Ni-BZY | BCY | Fe cell, the role of each electrode must be distinguished as both Ni and Fe are catalysts for ammonia electrosynthesis. An electrolyte-supported Pt | BCY | Fe cell was tested under the same conditions as those used for the electrode-supported cells. The highest ammonia formation rate was 8.8×10^{-11} mol s^{-1} cm^{-2} at −1.0 V and 9 mA cm^{-2} (Figure S5), which is 2 orders of magnitude lower than that obtained with the electrode-supported cells. Thus, the potential effect of catalytic or electrochemical ammonia synthesis reactions at the Fe anode can be considered negligible; ammonia is predominantly formed at the Ni-BZY cathode, as intended. Although Ni is less commonly used as a catalyst for ammonia synthesis, its combination with barium-based perovskites has led to a promotional effect and to ammonia synthesis rates 10 times higher than that of pure Ni.[30] It is also noted that when used as an anode, Fe is poor at dissociating hydrogen into protons. However, it appears that when implemented into electrode-supported cells, the improved interfacial contact outweighs the effects of poor hydrogen oxidation.

2.4. Analysis of Rate Enhancement. From the results of ammonia electrosynthesis, the following were observed: (1) the difference in ammonia formation rate between the two cells is greater than the difference in current density; (2) the ammonia formation rate increases exponentially and non-Faradaically at low applied voltages; and (3) ammonia formation saturates at higher applied voltages.

Typically, ammonia synthesis proceeds by either a dissociative mechanism or an associative mechanism, as shown in Table 2. The dissociative mechanism is considered

Table 2. Dissociative and Associative Mechanisms for Ammonia Synthesis

dissociative mechanism		associative mechanism	
$N_2 + * \rightarrow N_2*$	R1	$N_2* + 3H^+ + 3e^- \rightarrow N_2H_3*$	R6
$N_2* + * \rightarrow 2N*$	R2	$N_2H_3* \rightarrow N* + NH_3$	R7
$H_2 + 2* \rightarrow 2H*$	R3	$N* + 3H^+ + 3e^- \rightarrow NH_3*$	R8
$N* + 3H* \rightarrow NH_3* + 3*$	R4	$NH_3* \rightarrow NH_3 + *$	R9
$NH_3* \rightarrow NH_3 + *$	R5		

in the catalytic Haber−Bosch reaction,[31] while the associative mechanism is thought to proceed in electrochemical reactions.[32] Here, as the proton flux through the electrolyte does not appear to be the rate-limiting factor for ammonia formation, we assume that the reaction is closer to a catalytic reaction and consider the dissociative mechanism hereon. Indeed, our group previously showed using deuterium isotopic analysis that most of the hydrogen atoms that constitute the produced ammonia are from the cathode gas feed.[33] In the dissociative mechanism, the dissociation of the N_2 triple bond (step 2) has been shown to be the rate-limiting step.[31] Adequately high temperatures are typically required for bond dissociation; however, the dissociation can be aided electrochemically as well. In EPOC, it has been reported that electron backdonation from the catalyst to the π_{2p}* orbital of an adsorbed N_2 molecule can aid its dissociation.[12]

Based on the dissociative mechanism, it is thought that the following reactions occur in Regions 1 and 2, as shown in Figure 5. At lower applied voltages, it is thought that the

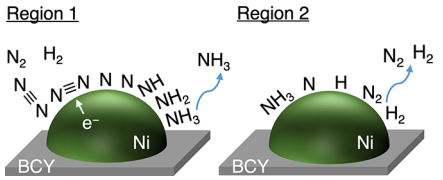

Figure 5. Schematic of reactions taking place in Regions 1 and Region 2. Region 1: electrochemical promotion of ammonia formation; Region 2: simultaneous forward ammonia synthesis reaction and backward ammonia decomposition reaction.

exponential increase in ammonia formation rate seen in Region 1 is due to electron backdonation to the adsorbed N≡N, promoting step R2 (Table 2). Indeed, such exponential behavior has been reported in electrochemically promoted catalytic reactions, as extensively studied by Vayenas and co-workers[11,12] The promoted formation rate has been described by $r_{NH3}/r_{NH3,OCV} = e^{\alpha F \Delta V/RT}$, where $r_{NH3,OCV}$ is the ammonia formation rate at OCV; α is the charge transfer coefficient ($\alpha <$ 1 for electrophilic reactions); ΔV is the applied voltage; and R is the gas constant.[12] At higher applied voltages, in Region 2, there appears to be an additional effect of the backward ammonia decomposition reaction ($NH_3 \rightarrow \frac{1}{2}N_2 + \frac{3}{2}H_2$), in addition to the forward ammonia synthesis reaction. Such decomposition has also been reported in catalytic ammonia synthesis reactions.[3] For further discussion of the mechanism and reaction intermediates, isotopic mixing and in situ infrared spectroscopy studies may be necessary.

Figure 6 shows how the highest ammonia formation rate reported in this study compares with those previously reported using PCECs with a mixed N_2/H_2 cathodic gas feed. A full data

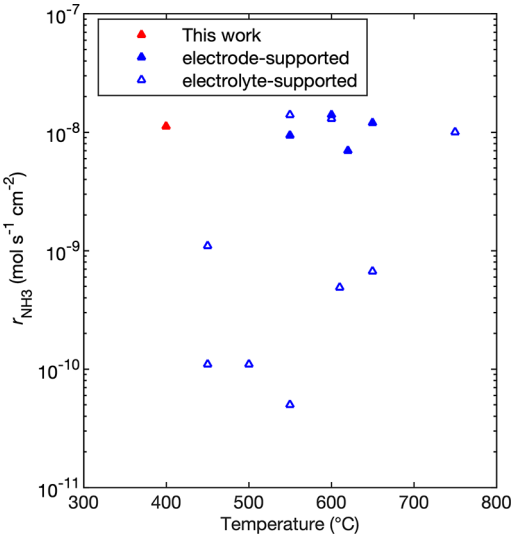

Figure 6. Comparison of electrochemical ammonia formation rates achieved in this work (red filled triangle) and in literature at different temperatures using PCECs with a mixed N_2/H_2 cathodic gas feed.[6−10,21,34] Works are categorized by cell support type (filled symbols for electrode-supported cells; open symbols for electrolyte-supported cells). The full data set is given in Table S1.

https://doi.org/10.1021/acsomega.3c04478
ACS Omega 2023, 8, 40299−40308

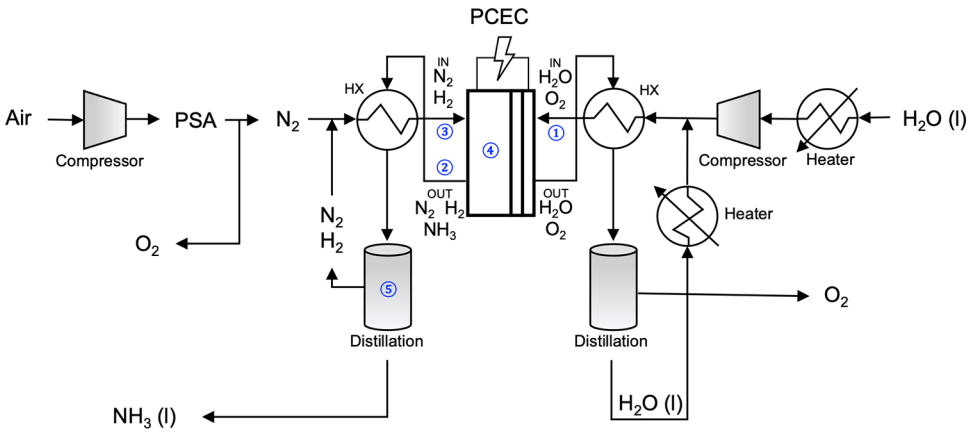

Figure 7. Schematic of a proposed ammonia electrosynthesis system that combines water electrolysis and ammonia electrosynthesis, with a recycling system to use the hydrogen byproduct.

set can be found in Table S1. Higher ammonia formation rates up to 1.5×10^{-8} mol s^{-1} cm^{-2} have been reported when using a mixed N_2/H_2 cathodic gas feed, enabling electrochemical promotion, but such high values have only been reported at 550 °C and above. Furthermore, although Ni-BZY had been widely used as an electrode support and Ni as a catalyst for ammonia electrosynthesis, its use as a cathode material had not led to such high ammonia formation rates at intermediate temperatures. In this work, high ammonia formation rates on the order of 10^{-8} mol s^{-1} cm^{-2} were achieved at 400 °C using a noble-metal-free Ni-BZY cathode catalyst, which corresponds to a 10-fold improvement in ammonia formation rate compared to previously reported works with a mixed N_2/H_2 cathodic gas feed below 500 °C, and to a reduction of the operating temperature by about 150 °C compared to studies reporting similarly high ammonia formation rates in similar conditions. It is thought that when sufficient cathodic polarization to facilitate N_2 dissociation is achieved, the electrochemical promotion of catalysis can be enabled, even at lower temperatures.

2.5. Proposed Ammonia Electrosynthesis System. Through our experimental results, we demonstrated the viability of conducting ammonia electrosynthesis at 400 °C in a mixed cathodic atmosphere of N_2/H_2. Based on this work, future prospects include the development of a novel ammonia electrosynthesis system that combines direct ammonia electrosynthesis from water with the electrochemical promotion of catalysis, enabled by introducing a hydrogen recycling stream. A schematic of our proposed system is shown in Figure 7. The concept is as follows, corresponding to the numbered labels in Figure 7: (1) water electrolysis is conducted at the anode side; (2) hydrogen is produced as a byproduct at the cathode side; (3) hydrogen is recycled to the cathode inlet stream, along with nitrogen from air to form a mixed N_2/H_2 cathode feed; (4) ammonia formation is electrochemically promoted at the cathode; and (5) produced ammonia is separated from the N_2/H_2 recycling stream by cooling under pressurized conditions. To maintain the material balance of hydrogen in the system, only sufficient H_2O to replenish the produced NH_3 is newly fed to the anode side.

This combined system has the potential for fast ammonia production using an energy-efficient PCEC, based on electrochemically promoted ammonia synthesis enabled at intermediate temperatures. By introducing a recycling system, hydrogen can be fed to the cathode side without requiring a separate cell stack for hydrogen production, minimizing the space and materials required. In terms of practicality, while water electrolysis using PCECs is more common at high temperatures above 500 °C, it has also been demonstrated at temperatures as low as 350 °C, with a high current density of 0.9 A cm^{-2} reported at 400 °C.[35] Furthermore, the produced ammonia can be kept separate from water throughout the process, eliminating the need for an energetically costly water−ammonia separation unit.[36] The main separation required is between ammonia and the mixed N_2/H_2 gas feed, which can be easily conducted by lowering the temperature under mildly pressurized conditions.

3. CONCLUSIONS

Ammonia electrosynthesis was conducted in a single-chamber reactor at intermediate temperatures using electrode-supported Ni-BZY | BCY | Pt and Ni-BZY | BCY | Fe cells. A high ammonia formation rate of 1.1×10^{-8} mol s^{-1} cm^{-2} was achieved at 400 °C using the Ni-BZY cathode in 50% N_2/50% H_2 at an applied voltage of −1.25 V. Our results indicate that high ammonia formation rates can indeed be achieved with PCECs at intermediate temperatures even without noble metals, provided that sufficient cathodic polarization is applied to enable the electrochemical promotion of catalysis. By implementing electrode-supported cells with a thin spin-coated electrolyte, the Ohmic resistance was minimized, with a further reduction due to improved contact at the anode−electrolyte interface. This improvement likely allowed for sufficient polarization to be applied to the cathode rather than being consumed by the Ohmic and anodic resistances, enabling electron backdonation from the Ni-BZY catalyst to the adsorbed N_2 molecules and facilitating N_2 dissociation, ultimately leading to a more pronounced EPOC effect. Moreover, by testing the cells in a single-chamber reactor with a mixed N_2/H_2 gas feed, hydrogen was sufficiently supplied without being limited by the flux of protons through the electrolyte. Based on the enhanced ammonia synthesis in a mixed N_2/H_2 atmosphere, a novel ammonia electrosynthesis system is proposed in which direct ammonia electrosynthesis from water and nitrogen is combined with hydrogen recycling at the cathode side to promote ammonia formation. Through cell design and analysis, this work demonstrates the viability of intermediate temperature ammonia electrosynthesis using PCECs and provides insight into the development of an energy-efficient ammonia electrosynthesis system.

https://doi.org/10.1021/acsomega.3c04478
ACS Omega 2023, 8, 40299−40308

4. METHODS

4.1. Materials Synthesis. BCY was synthesized by the coprecipitation method as described previously,[8] using precursors of $Ba(NO_3)_2$ (99.0% purity), $Ce(NO_3)_3{\cdot}6H_2O$ (99.99% purity), $(NH_4)_2C_2O_4{\cdot}6H_2O$ (99.5% purity; all from Kanto Chemical Co., Japan), and $Y(NO_3)_3{\cdot}6H_2O$ (99.99% purity; Junsei Chemical Co., Japan). In brief, a 0.2 M solution containing the cation precursors was added dropwise into a 0.2 M $(NH_4)_2C_2O_4{\cdot}6H_2O$ solution while stirring, to form a precipitate. The precipitate was filtered and dried, before calcining at 800 °C in air, and then at 1200 °C in air. The calcined BCY powder was ball-milled in ethanol and then sieved to obtain powders finer than 75 μm. Phase formation of the BCY powder was verified via XRD.

4.2. Fabrication of Electrode-Supported Cells. 60 wt % NiO (99.0% purity; Wako Pure Chemical Corp., Japan) and 40 wt % $BaZr_{0.8}Y_{0.2}O_{3-\delta}$ (BZY; KCeraCell, Korea) were combined by ball-milling in ethanol. After evaporation, PMMA (99.9% purity; Tokyo Chemical Industry, Co., Japan) dispersed in acetone (6 wt %) was ground into the NiO-BZY mixture (0.5 wt % PMMA in powder mixture) to serve as a binder and pore-former. NiO-BZY-PMMA powders were pelletized into discs 10 mm in diameter by uniaxial pressing at 4 t cm^{-2}, followed by cold isostatic pressing at 160 MPa. The BCY electrolyte was deposited onto the green cermet pellet via spin-coating a slurry made from BCY powder (32 wt %), ethanol (65 wt %), ethyl cellulose (1 wt %; binder; 48.0−49.5% ethoxy content; Kanto Chemical Co., Japan), Nonion OP-83 RAT sorbitan sesquioleate (1 wt %; dispersant; NOF Co., Japan), and dibutyl phthalate (1 wt %; plasticizer; 99.5% purity; Kanto Chemical Co., Japan). The cathode and electrolyte were cosintered at 1400 °C in air for 7 h.

The doctor-blading method was used to form porous anodes, as described previously.[8] A different slurry was made from α-terpineol (72 wt %; 98% purity; Wako Pure Chemical Corp., Japan), ethyl cellulose (10 wt %), Nonion OP-83 RAT sorbitan sesquioleate (6 wt %), dibutyl phthalate (6 wt %), and PMMA (7 wt %). The slurry was mixed with α-Fe_2O_3 (98% purity; Wako Pure Chemical Corp., Japan), deposited onto the electrolyte, and calcined at 900 °C in air to form Fe anodes. Porous Pt paste (Tanaka Kikinzoku Kogyo, Japan) was used as purchased and calcined at 900 °C in air to form Pt anodes. The active cell area was 0.28 cm^2 for the electrode-supported cells.

4.3. Fabrication of Electrolyte-Supported Cells. BCY powder was pelletized into discs 10 mm in diameter by uniaxial pressing at 4 t cm^{-2} followed by cold isostatic pressing at 180 MPa. The resulting pellets were sintered at 1600 °C in air while covered in sacrificial BCY powder to prevent barium vaporization. The relative densities of the sintered electrolyte pellets, compared to a theoretical value,[37] were over 90%. The doctor-blading method was used to form both electrodes as described above. Either Fe or Pt was used as the working electrode and Pt as the counter electrode. The active cell area was 0.13 cm^2 for electrolyte-supported cells.

4.4. Characterization. XRD (Mini Flex 600; Rigaku, Japan) was used to examine the phase purities of the as-prepared BCY powder, cosintered BCY electrolyte, and reduced Ni-BZY support. Cell cross sections were osmium-coated and visualized via FE-SEM (JSM-7500F; JEOL, Japan) after electrochemical measurements.

4.5. Electrochemical Measurements. Au mesh and wires (Nilaco Corp., Japan) were used as current collectors and held against the cell by using a ceramic rig. Electrochemical measurements were conducted in a single-chamber reactor (Figure 8) consisting of a quartz tube with a volume of approximately 200 cm^3 and an internal diameter of ø2.2 cm (cross-sectional area of 3.8 cm^2). Cells were reduced at 700 °C in 20% H_2/Ar. Ammonia synthesis was conducted at 400 °C, and inlet gases (dry 50% N_2/50% H_2) were fed at a fixed flow rate of 200 sccm at atmospheric pressure. The inlet gas feed ratio of 50% N_2/50% H_2 was selected based on a previous study, which considered the effect of the cathode gas feed ratio on the ammonia formation rate under cofed N_2/H_2 conditions.[8] N_2 gas of G1 grade (>99.99995% purity) was used. Potentiostatic measurements were conducted using an Autolab PGSTAT128 (Metrohm Autolab B.V., Netherlands) in a two-electrode configuration. All impedance spectra were taken in the frequency range 10^5−10^{-1} Hz with 10 points per decade and an amplitude of 10 mV. Impedance spectra were fitted by the complex nonlinear least-squares method using RelaxIS software (rhd instruments, Germany).

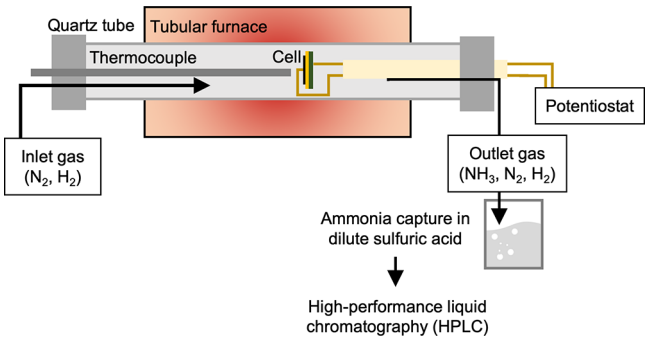

Figure 8. Schematic of the single-chamber electrochemical testing unit.

4.6. Ammonia Formation. To capture the gaseous ammonia formed, we bubbled the outlet gas into a dilute 0.01 mM sulfuric acid solution. For each parameter tested, the wait time for stabilization was 20 min before collecting the outlet gas in 10 min intervals over a 20 min period. The capture solutions were analyzed via high performance liquid chromatography (HPLC; Extrema; Jasco, Japan) equipped with electrical conductivity detection (CD-200, Shodex, Japan) to quantify the ammonia produced using the HPLC calibration curves shown in Figures S6 and S7.

■ ASSOCIATED CONTENT

Supporting Information

The Supporting Information is available free of charge at https://pubs.acs.org/doi/10.1021/acsomega.3c04478.

Additional electrochemical data for validation (blank test, reversibility test, stability test, reproducibility test, and reference test), data set for comparison to literature, and HPLC calibration curves (PDF)

■ AUTHOR INFORMATION

Corresponding Author

Junichiro Otomo − *Department of Transdisciplinary Science and Engineering, School of Environment and Society, Tokyo Institute of Technology, Meguro-ku, Tokyo 152-8550, Japan;* orcid.org/0000-0002-3179-8284; Email: otomo@tse.ens.titech.ac.jp

https://doi.org/10.1021/acsomega.3c04478
ACS Omega 2023, 8, 40299−40308

Author

Moe Okazaki − *Department of Environment Systems, Graduate School of Frontier Sciences, The University of Tokyo, Kashiwa-shi, Chiba 277-8561, Japan;* orcid.org/0000-0003-3579-5571

Complete contact information is available at: https://pubs.acs.org/10.1021/acsomega.3c04478

Author Contributions

M.O.: writing−original draft preparation, investigation, formal analysis, methodology, data curation, validation; J.O.: conceptualization, methodology, writing−reviewing and editing, supervision. All authors have given approval to the final version of the manuscript.

Funding

This work was funded by JSPS KAKENHI Grant Numbers JP21H04938 and JP22KJ0807.

Notes

The authors declare no competing financial interest.

■ ACKNOWLEDGMENTS

This work was supported by JSPS KAKENHI Grant Numbers JP21H04938 and JP22KJ0807, from the Japan Society for the Promotion of Science. The authors thank the Materials Division, Open Facility Center, Tokyo Institute of Technology for use of their XRD and FE-SEM facilities.

■ ABBREVIATIONS

ASR, area-specific resistance; CPE, constant phase element; EIS, electrochemical impedance spectroscopy; EPMA, electron probe microanalysis; EPOC, electrochemical promotion of catalysis; FE, Faradaic efficiency; FE-SEM, field emission scanning electron microscopy; HPLC, high-performance liquid chromatography; OCV, open-circuit voltage; PCEC, protonic ceramic electrolysis cell; PCFC, protonic ceramic fuel cell; XRD, X-ray diffraction

■ REFERENCES

(1) Bicer, Y.; Dincer, I. Life Cycle Assessment of Ammonia Utilization in City Transportation and Power Generation. *J. Cleaner Prod.* **2018**, *170*, 1594−1601.

(2) Erisman, J. W.; Sutton, M. A.; Galloway, J.; Klimont, Z.; Winiwarter, W. How a Century of Ammonia Synthesis Changed the World. *Nat. Geosci.* **2008**, *1*, 636−639.

(3) Aika, K.; Ozaki, A. Kinetics and Isotope Effect of Ammonia Synthesis over an Unpromoted Iron Catalyst. *J. Catal.* **1969**, *13*, 232−237.

(4) Qing, G.; Ghazfar, R.; Jackowski, S. T.; Habibzadeh, F.; Ashtiani, M. M.; Chen, C. P.; Smith, M. R.; Hamann, T. W. Recent Advances and Challenges of Electrocatalytic N_2 Reduction to Ammonia. *Chem. Rev.* **2020**, *120*, 5437−5516.

(5) Martín, A. J.; Shinagawa, T.; Pérez-Ramírez, J. Electrocatalytic Reduction of Nitrogen: From Haber-Bosch to Ammonia Artificial Leaf. *Chem* **2019**, *5*, 263−283.

(6) Vasileiou, E.; Kyriakou, V.; Garagounis, I.; Vourros, A.; Manerbino, A.; Coors, W. G.; Stoukides, M. Electrochemical Enhancement of Ammonia Synthesis in a $BaZr_{0.7}Ce_{0.2}Y_{0.1}O_{2.9}$ Solid Electrolyte Cell. *Solid State Ion* **2016**, *288*, 357−362.

(7) Ouzounidou, M.; Skodra, A.; Kokkofitis, C.; Stoukides, M. Catalytic and Electrocatalytic Synthesis of NH_3 in a H+ Conducting Cell by Using an Industrial Fe Catalyst. *Solid State Ion* **2007**, *178*, 153−159.

(8) Li, C.; Matsuo, H.; Otomo, J. Effective Electrode Design and the Reaction Mechanism for Electrochemical Promotion of Ammonia Synthesis Using Fe-Based Electrode. *Sustainable Energy Fuels* **2021**, *5*, 188−198.

(9) Kosaka, F.; Nakamura, T.; Oikawa, A.; Otomo, J. Electrochemical Acceleration of Ammonia Synthesis on Fe-Based Alkali-Promoted Electrocatalyst with Proton Conducting Solid Electrolyte. *ACS Sustainable Chem. Eng.* **2017**, *5*, 10439−10446.

(10) Vasileiou, E.; Kyriakou, V.; Garagounis, I.; Vourros, A.; Stoukides, M. Ammonia Synthesis at Atmospheric Pressure in a $BaCe_{0.2}Zr_{0.7}Y_{0.1}O_{2.9}$ Solid Electrolyte Cell. *Solid State Ion* **2015**, *275*, 110−116.

(11) Vernoux, P.; Lizarraga, L.; Tsampas, M. N.; Sapountzi, F. M.; De Lucas-Consuegra, A.; Valverde, J. L.; Souentie, S.; Vayenas, C. G.; Tsiplakides, D.; Balomenou, S.; Baranova, E. A. Ionically Conducting Ceramics as Active Catalyst Supports. *Chem. Rev.* **2013**, *113*, 8192−8260.

(12) Vayenas, C. G.; Koutsodontis, C. G. Non-Faradaic Electrochemical Activation of Catalysis. *J. Chem. Phys.* **2008**, *128*, 182506−1825013.

(13) Vayenas, G. The Effect of Electrochemical Oxygen Pumping on the Rate and Selectivity of Ethylene Oxidation on Polycrystalline. *J. Catal.* **1981**, *70*, 137−146.

(14) Vayenas, C. G.; Bebelis, S.; Ladas, S. Dependence of Catalytic Rates on Catalyst Work Function. *Nature* **1990**, *343*, 625−627.

(15) Fernandez, C. A.; Hortance, N. M.; Liu, Y. H.; Lim, J.; Hatzell, K. B.; Hatzell, M. C. Opportunities for Intermediate Temperature Renewable Ammonia Electrosynthesis. *J. Mater. Chem. A* **2020**, *8*, 15591−15606.

(16) Choi, S.; Kucharczyk, C. J.; Liang, Y.; Zhang, X.; Takeuchi, I.; Il Ji, H.; Haile, S. M. Exceptional Power Density and Stability at Intermediate Temperatures in Protonic Ceramic Fuel Cells. *Nat. Energy* **2018**, *3*, 202−210.

(17) Fabbri, E.; Pergolesi, D.; Traversa, E. Materials Challenges toward Proton-Conducting Oxide Fuel Cells: A Critical Review. *Chem. Soc. Rev.* **2010**, *39*, 4355−4369.

(18) Kim, H.; Chung, Y. S.; Kim, T.; Yoon, H.; Sung, J. G.; Jung, H. K.; Kim, W. B.; Sammes, L. B.; Chung, J. S. Ru-Doped Barium Strontium Titanates of the Cathode for the Electrochemical Synthesis of Ammonia. *Solid State Ion* **2019**, *339*, No. 115010.

(19) Wang, W. B.; Cao, X. B.; Gao, W. J.; Zhang, F.; Wang, H. T.; Ma, G. L. Ammonia Synthesis at Atmospheric Pressure Using a Reactor with Thin Solid Electrolyte $BaCe_{0.85}Y_{0.15}O_{3-\alpha}$ Membrane. *J. Membr. Sci.* **2010**, *360*, 397−403.

(20) Li, M.; Hua, B.; Wu, W.; Wang, L. C.; Ding, Y.; Welander, M. M.; Walker, R. A.; Ding, D. Activating Nano-Bulk Interplays for Sustainable Ammonia Electrosynthesis. *Mater. Today* **2022**, *60*, 31−40.

(21) Okazaki, M.; Otomo, J. Iron-Based Electrode Structures for Ammonia Electrosynthesis Cells with Proton-Conducting Ceramic Electrolytes. *ECS Trans.* **2022**, *109* (13), 3−12.

(22) Giannici, F.; Chiara, A.; Canu, G.; Longo, A.; Martorana, A. Interface Solid-State Reactions in $La_{0.8}Sr_{0.2}MnO_3/Ce_{0.8}Sm_{0.2}O_2$ and $La_{0.8}Sr_{0.2}MnO_3/BaCe_{0.9}Y_{0.1}O_3$ Disclosed by X-Ray Microspectroscopy. *ACS Appl. Energy Mater.* **2019**, *2*, 3204−3210.

(23) Sumi, H.; Shimada, H.; Watanabe, K.; Yamaguchi, Y.; Nomura, K.; Mizutani, Y.; Okuyama, Y. External Current Dependence of Polarization Resistances for Reversible Solid Oxide and Protonic Ceramic Cells with Current Leakage. *ACS Appl. Energy Mater.* **2023**, *6*, 1853−1861.

(24) Sumi, H.; Shimada, H.; Yamaguchi, Y.; Mizutani, Y.; Okuyama, Y.; Amezawa, K. Comparison of Electrochemical Impedance Spectra for Electrolyte-Supported Solid Oxide Fuel Cells (SOFCs) and Protonic Ceramic Fuel Cells (PCFCs). *Sci. Rep.* **2021**, *11* (1), 10622.

(25) Fleig, J.; Schmid, A.; Rupp, G. M.; Slouka, C.; Navickas, E.; Andrejs, L.; Hutter, H.; Volgger, L.; Nenning, A. The Chemical Capacitance as a Fingerprint of Defect Chemistry in Mixed Conducting Oxides. *Acta Chim. Slov.* **2016**, *63*, 509−518.

(26) Shimada, H.; Yamaguchi, T.; Sumi, H.; Yamaguchi, Y.; Nomura, K.; Mizutani, Y.; Fujishiro, Y. A Key for Achieving Higher Open-Circuit Voltage in Protonic Ceramic Fuel Cells: Lowering

Interfacial Electrode Polarization. *ACS Appl. Energy Mater.* **2019**, *2*, 587−597.
(27) Tarutina, L. R.; Vdovin, G. K.; Lyagaeva, J. G.; Medvedev, D. A. $BaCe_{0.7}-XZr_{0.2}Y_{0.1}Fe_xO_{3-\delta}$ Derived from Proton-Conducting Electrolytes: A Way of Designing Chemically Compatible Cathodes for Solid Oxide Fuel Cells. *J. Alloys Compd.* **2020**, *831*, No. 154895.
(28) Wei, Z.; Wang, J.; Yu, X.; Li, Z.; Zhao, Y.; Chai, J. Study on Ce and Y Co-Doped $BaFeO_{3-\delta}$ Cubic Perovskite as Free-Cobalt Cathode for Proton-Conducting Solid Oxide Fuel Cells. *Int. J. Hydrogen Energy* **2021**, *46*, 23868−23878.
(29) Andersen, S. Z.; Čolić, V.; Yang, S.; Schwalbe, J. A.; Nielander, A. C.; McEnaney, J. M.; Enemark-Rasmussen, K.; Baker, J. G.; Singh, A. R.; Rohr, B. A.; Statt, M. J.; Blair, S. J.; Mezzavilla, S.; Kibsgaard, J.; Vesborg, P. C. K.; Cargnello, M.; Bent, S. F.; Jaramillo, T. F.; Stephens, I. E. L.; Nørskov, J. K.; Chorkendorff, I. A Rigorous Electrochemical Ammonia Synthesis Protocol with Quantitative Isotope Measurements. *Nature* **2019**, *570*, 504−508.
(30) Humphreys, J.; Lan, R.; Du, D.; Xu, W.; Tao, S. Promotion Effect of Proton-Conducting Oxide $BaZr_{0.1}Ce_{0.7}Y_{0.2}O_{3-\Delta}$ on the Catalytic Activity of Ni towards Ammonia Synthesis from Hydrogen and Nitrogen. *Int. J. Hydrogen Energy* **2018**, *43* (37), 17726−17736.
(31) Honkala, K.; Hellman, A.; Remediakis, I. N.; Logadottir, A.; Carlsson, A.; Dahl, S.; Christensen, C. H.; Norskov, J. K. Ammonia Synthesis from First-Principles Calculations. *Science* **2005**, *307*, 555−558.
(32) Skúlason, E.; Bligaard, T.; Gudmundsdóttir, S.; Studt, F.; Rossmeisl, J.; Abild-Pedersen, F.; Vegge, T.; Jónsson, H.; Nørskov, J. K. A Theoretical Evaluation of Possible Transition Metal Electro-Catalysts for N_2 Reduction. *Phys. Chem. Chem. Phys.* **2012**, *14* (3), 1235−1245.
(33) Li, C.-I.; Matsuo, H.; Otomo, J. Kinetic and Deuterium Isotope Analyses of Ammonia Electrochemical Synthesis. *RSC Adv.* **2021**, *11*, 17891−17900.
(34) Marnellos, G.; Stoukides, M. Ammonia Synthesis at Atmospheric Pressure. *Science* **1998**, *282*, 98−100.
(35) Bian, W.; Wu, W.; Wang, B.; Tang, W.; Zhou, M.; Jin, C.; Ding, H.; Fan, W.; Dong, Y.; Li, J.; Ding, D. Revitalizing Interface in Protonic Ceramic Cells by Acid Etch. *Nature* **2022**, *604*, 479−485.
(36) Wang, M.; Khan, M. A.; Mohsin, I.; Wicks, J.; Ip, A. H.; Sumon, K. Z.; Dinh, C. T.; Sargent, E. H.; Gates, I. D.; Kibria, M. G. Can Sustainable Ammonia Synthesis Pathways Compete with Fossil-Fuel Based Haber-Bosch Processes? *Energy Environ. Sci.* **2021**, *14*, 2535−2548.
(37) Takeuchi, K.; Loong, C. K.; Richardson, J. W.; Guan, J.; Dorris, S. E.; Balachandran, U. Crystal Structures and Phase Transitions in Y-Doped $BaCeO_3$: Their Dependence on Y Concentration and Hydrogen Doping. *Solid State Ion* **2000**, *138*, 63−77.

https://doi.org/10.1021/acsomega.3c04478
ACS Omega 2023, 8, 40299−40308